iScience

CellPress
OPEN ACCESS

Article

AMPKα2 is a skeletal muscle stem cell intrinsic regulator of myonuclear accretion

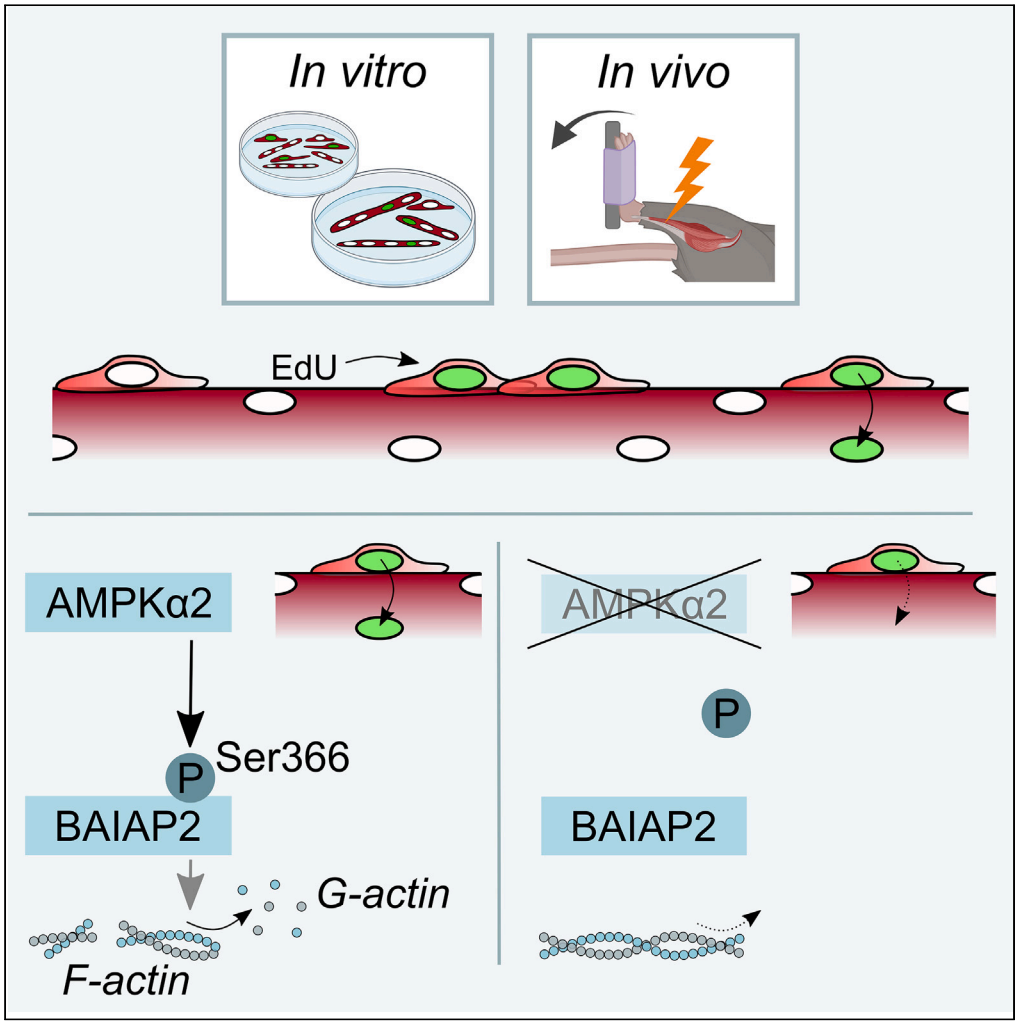

Anita Kneppers, Sabrina Ben Larbi, Marine Theret, ..., Julien Gondin, Kei Sakamoto, Rémi Mounier

remi.mounier@univ-lyon1.fr

Highlights

AMPKα2 is a MuSC-intrinsic physiological regulator of myonuclear accretion

AMPKα2 regulates MuSC fusion by phosphorylation of BAIAP2 at Ser366

AMPKα2 limits actin polymerization, to progress fusion beyond membrane apposition

Kneppers et al., iScience 26, 108343
December 15, 2023 © 2023
https://doi.org/10.1016/j.isci.2023.108343

iScience

CellPress
OPEN ACCESS

Article

AMPKα2 is a skeletal muscle stem cell intrinsic regulator of myonuclear accretion

Anita Kneppers,[1] Sabrina Ben Larbi,[1] Marine Theret,[1] Audrey Saugues,[1] Carole Dabadie,[1] Linda Gsaier,[1] Arnaud Ferry,[2,6] Philipp Rhein,[3,4] Julien Gondin,[1] Kei Sakamoto,[3,5] and Rémi Mounier[1,7,*]

SUMMARY

Due to the post-mitotic nature of skeletal muscle fibers, adult muscle maintenance relies on dedicated muscle stem cells (MuSCs). In most physiological contexts, MuSCs support myofiber homeostasis by contributing to myonuclear accretion, which requires a coordination of cell-type specific events between the myofiber and MuSCs. Here, we addressed the role of the kinase AMPKα2 in the coordination of these events supporting myonuclear accretion. We demonstrate that AMPKα2 deletion impairs skeletal muscle regeneration. Through *in vitro* assessments of MuSC myogenic fate and EdU-based cell tracing, we reveal a MuSC-specific role of AMPKα2 in the regulation of myonuclear accretion, which is mediated by phosphorylation of the non-metabolic substrate BAIAP2. Similar cell tracing *in vivo* shows that AMPKα2 knockout mice have a lower rate of myonuclear accretion during regeneration, and that MuSC-specific AMPKα2 deletion decreases myonuclear accretion in response to myofiber contraction. Together, this demonstrates that AMPKα2 is a MuSC-intrinsic regulator of myonuclear accretion.

INTRODUCTION

Skeletal muscle tissue constitutes approximately 45% of the total body weight in healthy humans, is a major determinant of the basal metabolic rate, and has well-recognized endocrine functions.[1,2] A low skeletal muscle mass is associated with metabolic disorders such as insulin resistance and type 2 diabetes, and is a risk factor for cardiovascular diseases and mortality,[3–5] illustrating the importance of skeletal muscle for whole body homeostasis. In addition, skeletal muscle quality and quantity are vital prerequisites for breathing, locomotion and performing daily tasks.[6] These functions are supported by the excitability and contractility of the myofibers, which are syncytia composed of hundreds of post-mitotic nuclei. Due to the post-mitotic nature of myofibers, adult muscle maintenance relies on dedicated skeletal muscle stem cells (MuSCs; a.k.a. satellite cells), which through their exit from quiescence, expansion, differentiation, and subsequent fusion, contribute to *de novo* myofiber formation after injury.[7]

Most commonly used models to study MuSC function invoke myofiber death by intramuscular injection with myotoxic agents, or by physical procedures such as freeze injury,[8] leading to a subsequent *de novo* myofiber formation. However, in humans complete *de novo* myofiber formation is exceedingly rare, since myofiber damage is usually contraction-induced and can lead to segmental myofiber necrosis.[9,10] As such, the recovery from myofiber damage in humans does not just rely on the fusion among MuSCs, but also relies on the fusion of MuSCs with pre-existing myofibers—*a process called "myonuclear accretion."* In addition to its role in the resolution of myofiber injury, myonuclear accretion was recently demonstrated to specifically contribute to adaptive remodeling in response to physical exercise.[11–13] Moreover, myonuclear accretion occurs continuously during life to support skeletal muscle homeostasis in both the young and adult organism.[14,15] Thus, while comon experimental models assess fusion among MuSCs during *de novo* myofiber formation, in most physiological contexts MuSCs support skeletal muscle homeostasis by their contribution to myonuclear accretion.

MuSC fusion is a tightly regulated process, which is illustrated by the array of proteins that play a critical role,[16] and the absolute requirement of muscle specific fusogens Myomaker (MYMK) and Myomixer (MYMX) to overcome the forces that prevent spontaneous membrane fusion.[17–20] Many of the components of the fusion machinery have been identified, but the physiological regulators of MuSC fusion remain largely unknown. Perhaps unsurprisingly, recent evidence points toward a distinct regulation of MuSC-MuSC fusion and myonuclear accretion.[21–23] For example, Eigler et al. proposed that Ca^{2+}/calmodulin-dependent protein kinase II (CaMKII) activation in growing myotubes (MT) specifically facilitates myonuclear accretion.[23] In addition, serum response factor (SRF)/cyclooxygenase-2 were shown to promote myonuclear

[1]Institut NeuroMyoGène, CNRS UMR 5261, INSERM U1315, Université Claude Bernard Lyon 1, Lyon, France
[2]Myology Center of Research, Association of Myology Institute, INSERM UMRS974, Sorbonne Université, Paris, France
[3]Nestlé Research, Société des Produits Nestlé S.A., EPFL Innovation Park, Lausanne, Switzerland
[4]School of Life Sciences, Ecole Polytechnique Fédérale de Lausanne (EPFL), EPFL Innovation Park, Lausanne, Switzerland
[5]Novo Nordisk Foundation Center for Basic Metabolic Research, University of Copenhagen, Copenhagen, Denmark
[6]Université Paris Cité, Paris, France
[7]Lead contact
*Correspondence: remi.mounier@univ-lyon1.fr
https://doi.org/10.1016/j.isci.2023.108343

accretion through the transcriptional regulation of the MuSC recruitment factor interleukin-4 (IL-4) in myofibers.[22] These studies illustrate that myonuclear accretion requires a coordination of cell-type specific events between the myofiber and MuSCs. However, the central molecular regulator that coordinates these events remains unidentified.

Physical exercise, involving repeated skeletal muscle contractions, is a robust physiological trigger of myonuclear accretion. Skeletal muscle contraction imposes an acute demand on myofiber Ca^{2+} fluxes and energy turnover. As such, we postulate that the key energy sensor and master regulator of cell metabolism "5′-AMP-activated protein kinase" (AMPK) may act as a central molecular regulator of myonuclear accretion. Interestingly, several pathways that distinctly regulate myonuclear accretion converge on AMPK. Indeed, AMPK is known to be regulated by Ca^{2+} signaling via Ca^{2+}/calmodulin-dependent protein kinase kinase 2 (CaMKK2). Furthermore, AMPK is a transcriptional and posttranscriptional regulator of peroxisome proliferative activated receptor, γ, coactivator 1 α (PGC1α),[24] which has recently been suggested to participate in the regulation of myonuclear accretion upon endurance type training.[25] Moreover, AMPK may be activated by nitric oxide,[26] which is released by MT upon mechanical tension and promotes myogenesis *in vitro*.[27,28]

AMPK is a heterotrimer composed of a catalytic subunit (α) and two regulatory subunits (β and γ).[24] The predominant AMPKα isoform in skeletal muscle is AMPKα2, which is also more robustly activated upon physical exercise.[29] We therefore addressed whether AMPKα2 has a role in the coordination of cell-type specific events supporting myonuclear accretion during the re-establishment of skeletal muscle homeostasis.

In uninjured, resting adult skeletal muscle, AMPKα2 is predominantly expressed in the myofibers. We demonstrate that AMPKα2 expression is progressively increased during MuSC-mediated myogenesis, and that MuSC-specific AMPKα2 deletion impairs skeletal muscle regeneration. Through *in vitro* assessments of the MuSC myogenic fate, we show that AMPKα2 knockout specifically decreases MuSC-myofiber fusion (i.e., myonuclear accretion). Furthermore, using 5 ethynyl 2′ deoxyuridine (EdU)-based cell tracing *in vitro*, we reveal a MuSC-specific role of AMPKα2 in the regulation of myonuclear accretion, which is mediated by the phosphorylation of the non-metabolic substrate BAR/IMD domain containing adaptor protein 2 (BAIAP2; a.k.a. IRSp53). Similar EdU-based cell tracing *in vivo* shows that AMPKα2 knockout mice have a lower rate of myonuclear accretion during regeneration, and that MuSC-specific AMPKα2 deletion decreases the relative rate of myonuclear accretion in response to myofiber contractions induced by neuromuscular electrical stimulation (NMES). Together, our analyses demonstrate that AMPKα2 is a MuSC-intrinsic regulator of myonuclear accretion.

RESULTS

AMPKα2 deletion impairs skeletal muscle regeneration

Using the integrated single-cell and single-nucleus transcriptomic database scMuscle,[30] we observed that AMPKα1 (*Prkaa1*) is expressed in various cell types present in the skeletal muscle, while AMPKα2 gene (*Prkaa2*) expression is largely confined to myonuclei (Figure S1A). Similarly, we have previously shown that AMPKα1 activity was present, while AMPKα2 activity is absent in quiescent MuSCs.[31] Interestingly, during *in vitro* myogenesis of FACS-sorted wild-type MuSCs, *Prkaa2* expression was progressively increased (Figure S1B). To assess AMPK activity during skeletal muscle regeneration *in vivo*, *tibialis anterior* (TA) muscles of wild-type mice were subjected to cardiotoxin (CTX)-induced injury (Figure 1A). Paralleling muscle cell-specific *in vitro* assessments, AMPKα2 activity was nearly absent at 2 days post injury (d.p.i.) when myofibers underwent a complete degeneration, and was gradually restored during myofiber regeneration at 7 and 14 d.p.i. (Figure 1B). Conversely, AMPKα1 activity was increased from 4 d.p.i. onward, coinciding with MuSC proliferation and immune cell infiltration (Figure 1C).

To study the role of AMPKα2 in skeletal muscle regeneration, mice lacking functional AMPKα2 (AMPKα2$^{-/-}$) were utilized. As anticipated, AMPKα2 activity was not detectable throughout the regenerative process (Figure 1B). Importantly, AMPKα1 activity did not display a compensatory increase in AMPKα2$^{-/-}$ TA (Figure 1C). Compared to wild-type control mice, AMPKα2$^{-/-}$ TA mass was unaffected before injury and at 2 and 4 d.p.i., but was lower at 7 and 14 d.p.i. (Figures 1D, S1C, S1D, and S1E), and returned back to normal by 28 d.p.i. (Figure S1F). In line, AMPKα2$^{-/-}$ muscle had a lower *in situ* force production at 14 d.p.i., while muscle fatigue remained unaffected (Figures 1E and S1G). Furthermore, AMPKα2$^{-/-}$ muscle contained a greater number of fibers expressing embryonic myosin heavy chain (eMyHC) at 14 d.p.i., whereas this maker of regeneration had returned to normal by 28 d.p.i. (Figures 1F and S1H), indicating an alteration in the kinetics of regeneration. Importantly, the number of Paired Box 7 (Pax7)$^{+}$ cells per fiber and the number of fibers per section were unaltered before injury, and at 28 d.p.i. (Figures S1I and S1J), demonstrating that myofiber re-formation and MuSC maintenance were unaffected in AMPKα2$^{-/-}$ TA.

To assess if the role of AMPKα2 during skeletal muscle regeneration is muscle cell-intrinsic, Pax7CreER$^{T2/+}$;AMPKα2$^{fl/fl}$ mice were treated with tamoxifen to induce AMPKα2 deletion in MuSCs and their progeny (AMPKα2$^{MuSC\Delta/\Delta}$), and then subjected to CTX-induced injury (Figures 1G and S1K). AMPKα2$^{MuSC\Delta/\Delta}$ mice had a lower relative TA mass, and a higher number of eMyHC^{+} fibers at 14 d.p.i. (Figures 1H, 1I, S1L, and S1M), whereas the number of Pax7^{+} cells remained unaffected (Figure S1N), indicating a muscle cell-intrinsic role of AMPKα2 during the progression of skeletal muscle regeneration.

AMPKα2 is a regulator of myoblast fusion

To dissect the muscle cell-intrinsic role of AMPKα2, myogenesis was modeled *in vitro* using FACS-sorted MuSCs (Figure S2A). EdU incorporation during the first 48 h of culture was unaffected while EdU incorporation into MuSC progeny (i.e., myoblasts) was lower in AMPKα2$^{-/-}$ cultures (Figures S2B and S2C), suggesting that AMPKα2 does not regulate MuSC activation but modulates the subsequent rate of proliferation. In parallel, myoblasts were induced to differentiate and fuse to form *in vitro* generated myofibers (i.e., MT) for up to 48 h, leading to a progressive increase in the fusion index of both AMPKα2$^{+/+}$ and AMPKα2$^{-/-}$ cultures (Figure 2A). However, at 48 h of *in vitro* myogenesis, the

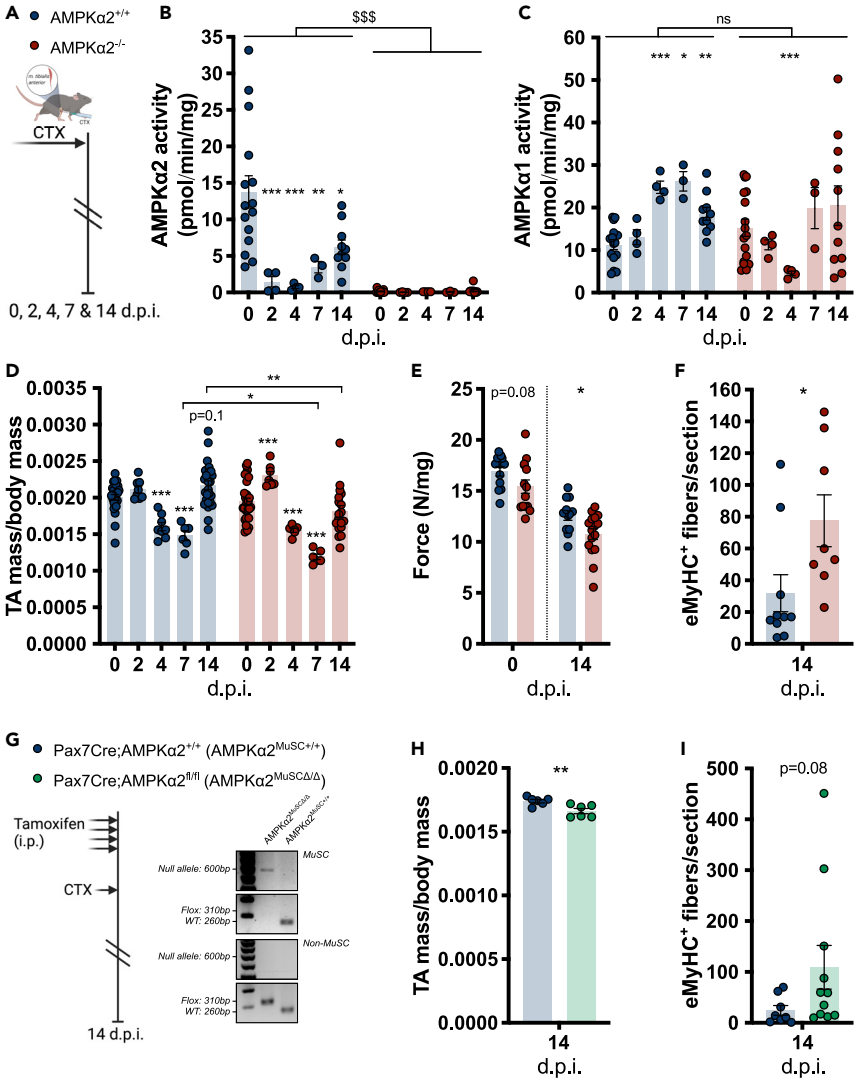

Figure 1. Role of AMPKα2 in skeletal muscle regeneration

Skeletal muscle regeneration in whole body AMPKα2$^{-/-}$ mice (A–F).

(A) Schematic of cardiotoxin (CTX)-induced skeletal muscle regeneration model and analysis endpoints at indicated days post injury (d.p.i.).

(B) Relative AMPKα2 activity during skeletal muscle regeneration.

(C) Relative AMPKα1 activity during skeletal muscle regeneration.

(D) Relative *tibialis anterior* (TA) mass during skeletal muscle regeneration.

(E) Relative *in situ* TA maximal force production before and 14 d.p.i.

(F) Number of eMyHC stained fibers per section at 14 d.p.i.

Skeletal muscle regeneration in mice after MuSC-specific AMPKα2 deletion (G–I).

(G) Schematic of tamoxifen-induced AMPKα2 deletion and subsequent CTX-based skeletal muscle regeneration model (left panel), and verification of MuSC-specific recombination in FACS-sorted MuSC (CD45/CD31/Sca1$^-$;CD34/α7int$^+$) versus non-MuSC (CD45/CD31/Sca1$^+$) extracted from hindlimb muscles of Pax7Cre; AMPKα2$^{+/+}$ (AMPKα2$^{+/+}$) and Pax7Cre; AMPKα2$^{fl/fl}$ (AMPKα2$^{\Delta/\Delta}$) mice at day 0 (i.e., 3 weeks after the first tamoxifen injection) (right panel).

(H) Relative TA mass at 14 d.p.i.

(I) Number of eMyHC stained fibers per section at 14 d.p.i. Bars represent mean ± SEM. Two-way ANOVA; $^{\$\$\$}p < 0.001$ genotype effect. Two-tailed, unpaired *t* test; *p < 0.05, **p < 0.01, ***p < 0.001, compared to 0 d.p.i., to AMPKα2$^{+/+}$ control, or between indicated bars. See also Figure S1.

fusion index remained lower in AMPKα2$^{-/-}$ cultures (Figure 2A). Conversely, treatment with a specific allosteric AMPK activator 991[32,33] increased the fusion index (Figure 2B), confirming a muscle cell-intrinsic role of AMPKα2 during myogenesis *in vitro*.

Metabolic alterations are known key drivers of MuSC differentiation.[34] Strikingly, the absence of AMPKα2—which is known to act as a metabolic sensor and coordinator of metabolic processes—did not affect the muscle cell-intrinsic differentiation capacity, as the number of

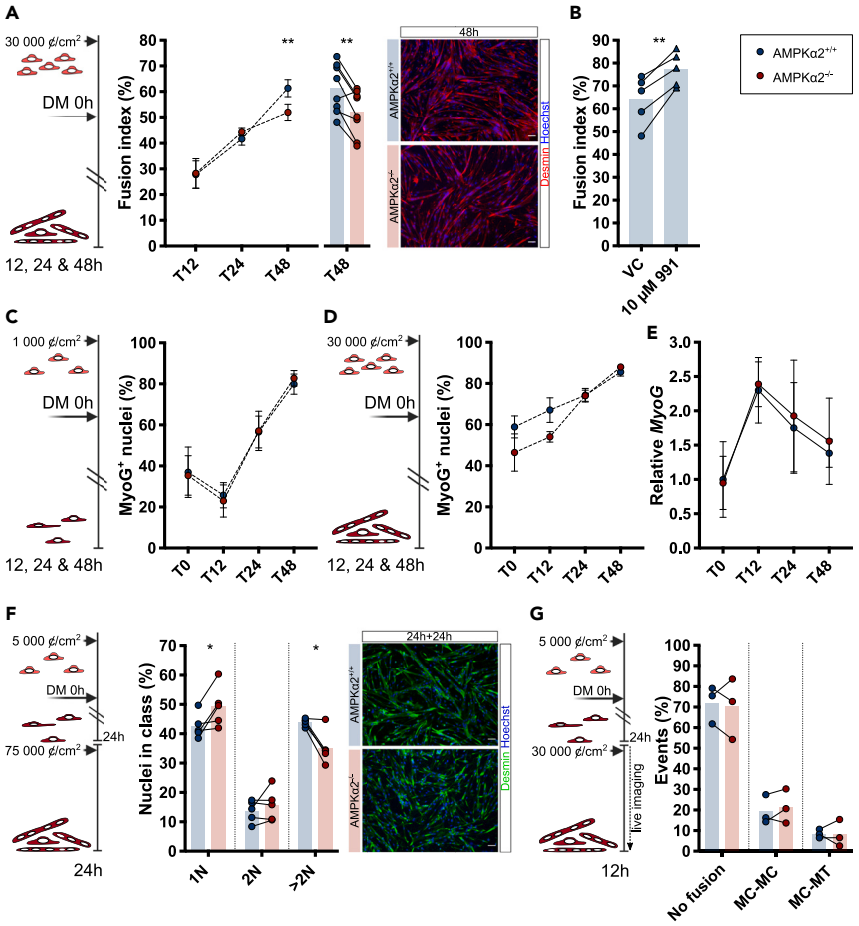

Figure 2. Role of AMPKα2 in the regulation of myoblast fusion *in vitro*

Left panels show schematic representation of experiments.

(A) Fusion index at indicated times of *in vitro* myogenesis, with insert of paired representation of the data at 48 h (T48, middle panel), and representative images (right panel).

(B) Fusion index after 48 h of *in vitro* myogenesis in cultures treated with 10 μM of the AMPK activator 991 or vehicle control (VC).

(C) Percentage of Myogenin (MyoG) stained nuclei at indicated times of differentiation in non-fusing cultures.

(D) Percentage MyoG stained nuclei at indicated times during *in vitro* myogenesis.

(E) Relative *MyoG* gene expression during *in vitro* myogenesis.

(F) Percentage of nuclei in cells with 1 nucleus (1N), 2 nuclei (2N) or >2 nuclei (>2N) after 24 h of fusion of pre-differentiated cells (middle panel), and representative images (right panel).

(G) Fusion events scored during 12 h of life imaging of fusing cultures of pre-differentiated cells. MC = myocytes, MT = myotubes. Bars represent mean. In line chart, dots represent mean ± SEM. Two-tailed, paired *t* test, *p < 0.05, **p < 0.01, compared to AMPKα2$^{+/+}$ control, or to VC. Length of white scale bar represents 50 μm. See also Figure S2.

unfused cells expressing Myogenin (MyoG) increased similarly in AMPKα2$^{+/+}$ and AMPKα2$^{-/-}$ cultures (Figure 2C). Moreover, the percentage of MyoG^{+} nuclei and *MyoG* gene expression were unaffected in AMPKα2$^{-/-}$ cultures during *in vitro* myogenesis (Figures 2D and 2E). Given the impaired fusion index despite unaffected differentiation in AMPKα2$^{-/-}$ cultures, we sought to assess the muscle cell-intrinsic fusion capacity of AMPKα2$^{-/-}$ cells. To this end, we differentiated myoblasts at low density to obtain differentiated mono-nucleated cells (i.e., myocytes (MC)), and subsequently cultured them at high density to isolate the process of fusion, as performed previously.[35] This assay resulted in a higher percentage of unfused cells (1N), and a lower fusion index in AMPKα2$^{-/-}$ cultures due to a reduced presence of nuclei in cells with >2 nuclei (Figure 2F). Interestingly, the occurrence of cells containing 2 nuclei—resulting from the fusion between two mononucleated cells—was unaffected in these cultures (Figure 2F), and in cultures subjected to the previously described protocol for *in vitro* myogenesis (Figure S2D). To directly assess the fusion between two mononucleated cells, fusion events were scored during 12 h live imaging of high-density cultured MC. We observed no difference in the rate of fusion between two mononucleated cells in AMPKα2$^{-/-}$ cultures (Figure 2G; Video S1), which suggests that the core fusion machinery is unaffected. Indeed, gene expression of the fusogens *Mymk* and *Mymx* were unaffected in AMPKα2$^{-/-}$ cultures (Figures S2E and S2F). Moreover, the motility parameters "velocity" and "directness," which influence the migration step of the fusion

process, were unaltered (Figure S2G; Video S2). Together, this shows that AMPKα2 is a regulator of myocyte fusion, specifically controlling the addition of nuclei to multinucleated MT.

AMPKα2 is a myocyte-intrinsic regulator of myonuclear accretion

The general paradigm is that during skeletal muscle development and regeneration, the initial establishment of myofibers by MuSC-MuSC fusion is followed by myonuclear accretion to support the formation of multinucleated cells.[36–38] To directly address the role of AMPKα2 in the regulation of myonuclear accretion *in vitro*, we performed co-culturing between MT and MC (Figure 3A; Videos S3, S4, S5, and S6). Myocyte-derived nuclei were traced by EdU incorporation at the myoblast stage, before initiation of co-culturing. After 24 h of incubation, EdU incorporation was similar between AMPKα2$^{+/+}$ and AMPKα2$^{-/-}$ MC (Figure 3B). However, co-culture of AMPKα2$^{-/-}$ MC with AMPKα2$^{+/+}$ MT resulted in a lower myonuclear accretion percentage ($p = 0.055$) and a higher percentage of unfused AMPKα2$^{-/-}$ MC (Figures 3C and 3D), whereas fusion of AMPKα2$^{-/-}$ MC with mononucleated cells was unaffected (data not shown). Moreover, treatment with the AMPK activator 991 increased the myonuclear accretion percentage in co-cultures with AMPKα2$^{+/+}$ MC, while this pro-fusion effect was absent in co-cultures with AMPKα2$^{-/-}$ MC (Figures 3E and 3F). Conversely, when MC were co-cultured with AMPKα2$^{-/-}$ MT the myonuclear accretion percentage and the percentage of unfused MC were unaffected (Figures S3A and S3B). In addition, the myonuclear accretion response to 991 treatment in co-cultures with AMPKα2$^{-/-}$ MT was similar to that in co-cultures with AMPKα2$^{+/+}$ MT (Figures S3C, S3D, 3E, and 3F). Together, this shows that AMPKα2 is a myocyte-intrinsic regulator of myonuclear accretion.

AMPKα2 regulates fusion through phosphorylation of BAIAP2 at Ser366

Chemical genetic screens have identified BAIAP2 as a novel target of AMPKα2.[39,40] An *in vitro* study using the mouse myoblast cell line C2C12 previously identified BAIAP2 as a negative regulator of myogenesis.[41] Moreover, a GWAS associated *BAIAP2* gene variants to weight loss in patients with chronic obstructive pulmonary disease (COPD)[42]—a disease linked with whole body and skeletal muscle wasting.[43] AMPKα2 directly phosphorylates BAIAP2 at Ser366,[39,40] which can regulate its cellular localization.[44] Moreover, regulation of the EPS8-BAIAP2 complex localization was recently linked to the progression of mammalian cell fusion.[45] We therefore explored the role of BAIAP2 in AMPKα2-mediated regulation of myonuclear accretion. *Baiap2* gene expression was strongly suppressed during *in vitro* myogenesis in both AMPKα2$^{+/+}$ and AMPKα2$^{-/-}$ cells (Figure S3E). However, BAIAP2^{WT} overexpression did not prevent myotube formation (Figures S3F and S3G). At 48 h of *in vitro* myogenesis, BAIAP2 localized at the tips of MT, and at sites of cell contact (Figures 3G and 3H). Importantly, transfection with the phospho-deficient mutant form BAIAP2^{S366A} prevented the pro-fusion effect induced by 991 (Figures 3I and S3H). Conversely, transfection with phosphomimetic mutant forms BAIAP2^{S366E} and BAIAP2^{S366D} completely rescued the fusion defect observed in AMPKα2$^{-/-}$ cultures (Figures 3J, S3I, S3J, and S3K). Together, this shows that AMPKα2 regulates fusion through the phosphorylation of BAIAP2 at Ser366.

Kast et al. previously demonstrated that BAIAP2 phosphorylation allows 14-3-3 binding, invoking a closed, autoinhibited conformation, which blocks its interactions with CDC42 and cytoskeletal effectors such as EPS8, and inhibits binding of BAIAP2 to cellular membranes.[44] Moreover, Rodríquez-Pérez et al. have shown that displacement of EPS8-BAIAP2 from membranes counteracts actin bundling and is required for the progression of fusion beyond membrane apposition.[45] We therefore assessed the relative abundance of filamentous (F) actin in AMPKα2$^{-/-}$ cultures, and found an increase in the F/G actin ratio (Figure 3K), which is in line with an inhibitory role for AMPKα2 in actin bundling through the phosphorylation of BAIAP2.

AMPKα2 is a MuSC-intrinsic regulator of myonuclear accretion in response to myofiber contractions induced by NMES

After CTX injury, MuSCs contribute to myofiber regeneration by MuSC-MuSC fusion and subsequent myonuclear accretion. To distinguish the MuSC contribution to these events *in vivo*, proliferating cells were traced by EdU labeling during the early (-1–5 d.p.i.) versus later phase of regeneration (5–14 d.p.i.) (Figure S4A). The timing of EdU labeling did not affect myonuclear number or localization (Figure S4B). Importantly, EdU labeling from 5 to 14 d.p.i. resulted in ~20% of EdU^{+} myonuclei, that predominantly localize at the periphery of the myofibers (Figures S4C and S4D), strongly suggesting their contribution through myonuclear accretion.[46]

Using EdU labeling from 5 to 14 d.p.i., we observed a lower number of EdU^{+} nuclei co-stained with the myofiber nucleus marker pericentriolar material 1 (PCM1) in AMPKα2$^{-/-}$ mice than in AMPKα2$^{+/+}$ controls at 14 d.p.i., indicating a lower rate of myonuclear accretion *in vivo* in the absence of AMPKα2 (Figures 4A and 4B). In contrast, we observed no difference in the number of EdU^{-} myofiber nuclei in AMPKα2$^{-/-}$ mice versus controls, showing that the first phase of regeneration including MuSC-MuSC fusion is unaffected *in vivo* (Figure 4B). Importantly, the total number of EdU^{+} nuclei below the basal lamina was reduced in AMPKα2$^{-/-}$ mice (Figure S4E). To explore the contribution of this MuSC expansion defect to alterations in the myonuclear accretion rate, we expressed the EdU^{+}/PCM1^{+} nuclei as a percentage of the total of EdU^{+} nuclei below the basal lamina. The resulting myonuclear accretion percentage is high (~70%) and unaffected in AMPKα2$^{-/-}$ mice (Figure 4C). This may suggest that the myonuclear accretion defect in 14 days regenerated muscle is primarily caused by impaired MuSC expansion in AMPKα2$^{-/-}$ mice, but alternatively, fusion defective MuSCs in AMPKα2$^{-/-}$ muscles may suppress later rounds of MuSC division.

To dissect the MuSC versus myofiber-specific roles of AMPKα2 in the regulation of myonuclear accretion, we sought to trigger myonuclear accretion *in vivo* without injuring the myofibers. A recent study showed that 6 sessions of individualized NMES increased the number of nuclei per myofiber without invoking signs of myofiber damage or regeneration.[47] We resolved the MuSC versus myofiber-specific roles of AMPKα2 by subjecting cell-type specific conditional knockout mice to this individualized NMES protocol, and directly assessed myonuclear accretion by EdU-based cell tracing throughout the protocol (Figure 4D). Maximal *in vivo* tetanic force did not differ between wild-type and AMPKα2$^{MuSC\Delta/\Delta}$ mice throughout the stimulation protocol (Figure S4F), imposing a similar relative stimulation load. Moreover, NMES

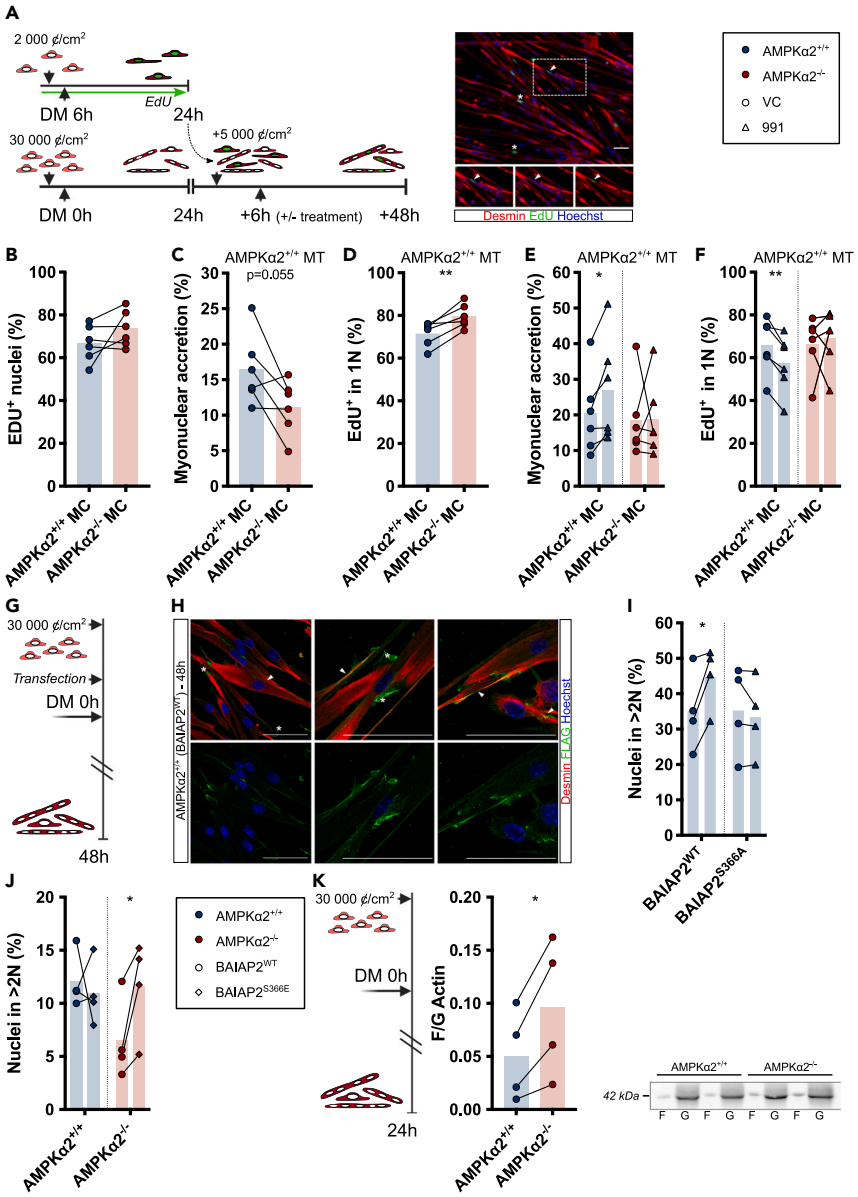

Figure 3. Myocyte-intrinsic regulation of *in vitro* myonuclear accretion by AMPKα2

(A) Schematic of co-culturing assay between 24 h differentiated MT and EdU-labeled pre-differentiated MC (left panel), and representative image (right panel). Arrow head indicates contribution of EdU$^+$ MC to myonuclear accretion, stars indicate mononucleated EdU$^+$ MC. Length of white scale bar represents 50 μm. MC = myocytes, MT = myotubes.

(B) Percentage EdU stained MC before start of co-cultures.

Co-cultures between AMPKα2$^{+/+}$ MT and AMPKα2$^{+/+}$ versus AMPKα2$^{-/-}$ MC (C–F).

(C) Percentage contribution of EdU$^+$ MC to myonuclear accretion after 48 h of co-culturing.

(D) Percentage EdU$^+$ MC that remain mononucleated after 48 h of co-culturing.

(E) Percentage contribution of EdU$^+$ MC to myonuclear accretion after 48 h of co-culturing with 10 μM of the AMPK activator 991 or vehicle control (VC).

(F) Percentage EdU$^+$ MC that remain mononucleated after 48 h of co-culturing with 10 μM 991 or VC.

(G) Schematic of transfection and subsequent *in vitro* myogenesis.

(H) Representative confocal images of BAIAP2 localization after 48 h of *in vitro* myogenesis of myoblasts transfected with BAIAP2^{WT}. Arrow head indicates BAIAP2 localization at the site of cell contact, stars indicate BAIAP2 localization at the tips of MT. Length of white scale bar represents 50 μm.

(I) Percentage of nuclei in cells with >2 nuclei (>2N) after 48 h of *in vitro* myogenesis of myoblasts transfected with BAIAP2^{WT} or BAIAP2^{S366A} with 10 μM of the AMPK activator 991 or VC.

(J) Percentage of nuclei in cells with >2 nuclei (>2N) after 48 h of *in vitro* myogenesis of myoblasts transfected with BAIAP2^{WT} or BAIAP2^{S366E}.

(K) Schematic representation of experiment (left panel), ratio between filamentous (F) and globular (G) actin (middle panel), and representative blot (right panel).

Bars represent mean. Two-tailed, paired *t* test, *p < 0.05, **p < 0.01, compared to AMPKα2$^{+/+}$ control, or to VC. See also Figure S3.

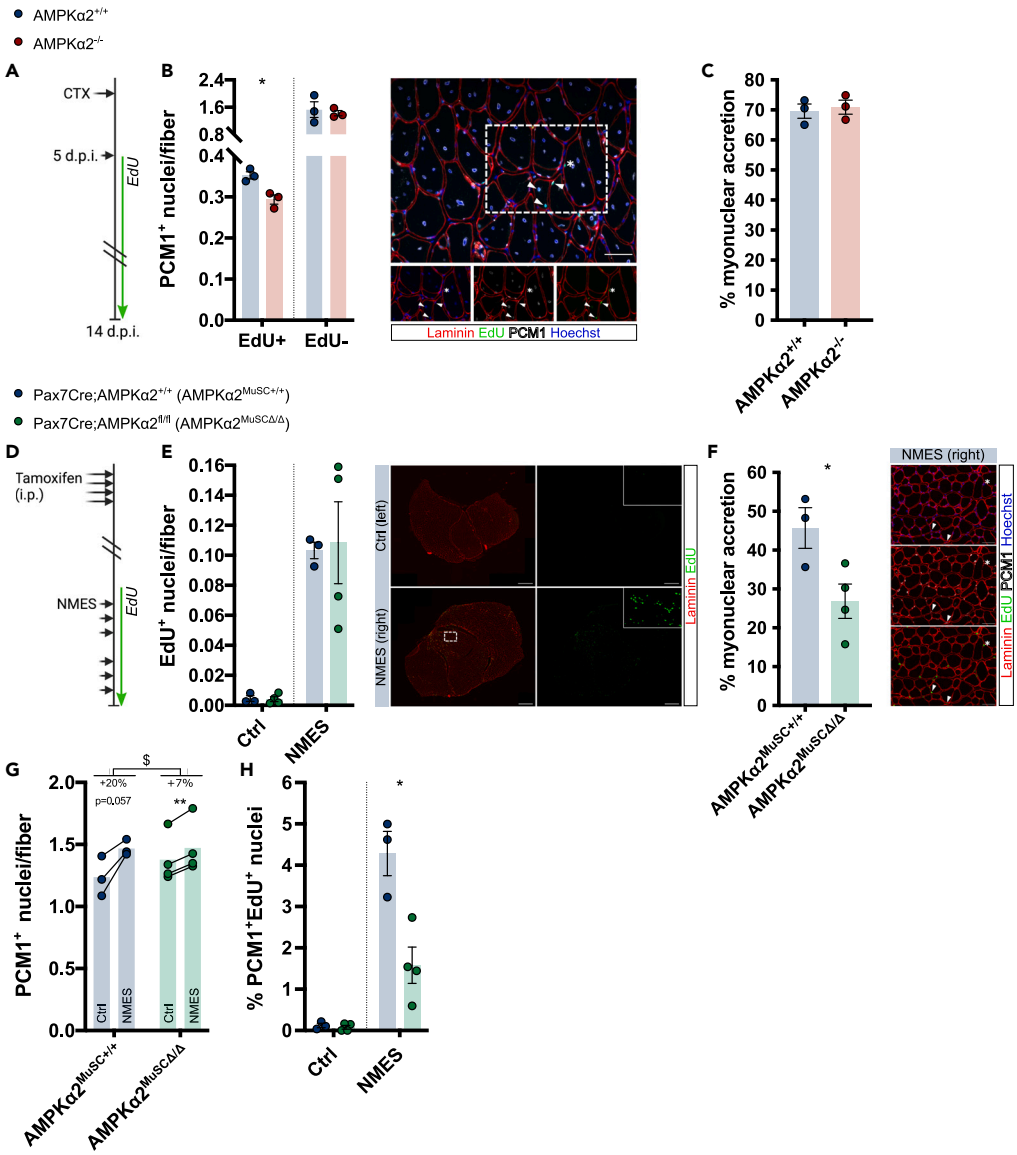

Figure 4. Role of AMPKα2 in the regulation of *in vivo* myonuclear accretion during regeneration and in response to muscle contraction induced by neuromuscular electrical stimulation (NMES)

EdU-based MuSC tracing in cardiotoxin (CTX)-based skeletal muscle regeneration model in whole body AMPKα2$^{-/-}$ mice (A–C).

(A) Schematic of experimental model, timing and duration of EdU-based tracing, and analysis endpoint at 14 days post injury (d.p.i.).

(B) Stratification of pericentriolar material 1 (PCM1)$^{+}$ nuclei per fiber by EdU staining at 14 d.p.i. (left panel), and representative image (right panel). Arrow heads indicate EdU^{+}/PCM1^{+} nuclei, star indicates EdU^{+}/PCM1^{-} nucleus. Length of white scale bar represents 50 μm.

(C) Percentage contribution of EdU^{+} nuclei below basal lamina to myonuclear accretion (i.e., are EdU^{+}/PCM1^{+}) at 14 d.p.i.

EdU-based MuSC tracing during neuromuscular electrical stimulation (NMES) in mice after MuSC-specific AMPKα2 deletion (D–G).

(D) Schematic of experimental model, and timing and duration of EdU-based tracing.

(E) Number of EdU^{+} nuclei below the basal lamina in muscle subjected to NMES versus contralateral control muscle (Ctrl) (left panel), and representative images (right panel). Length of white scale bar represents 500 μm. White dashed square indicates area presented in Figure 4F.

(F) Percentage contribution of EdU^{+} nuclei below basal lamina to myonuclear accretion after NMES (left panel), and representative images (right panel). Arrow heads indicate EdU^{+}/PCM1^{+} nuclei, star indicates EdU^{+}/PCM1^{-} nucleus. Length of white scale bar represents 50 μm.

(G) Number of PCM1^{+} nuclei per fiber in muscle subjected to NMES (NMES) versus contralateral control muscle (Ctrl).

(H) Percentage EdU^{+}/PCM1^{+} nuclei of PCM1^{+} nuclei in muscle subjected to NMES versus contralateral control muscle (Ctrl). Bars represent mean ± SEM. Two-tailed, unpaired *t* test. *p < 0.05, compared to AMPKα2$^{+/+}$ control. two-way ANOVA; $^{\$}$p < 0.05 genotype*NMES effect. Two-tailed, paired *t* test. **p < 0.01, compared to contralateral control muscle. See also Figure S4.

did not invoke signs of regeneration in either wild-type or AMPKα2$^{MuSC\Delta/\Delta}$ mice (Figure S4G). Strikingly, after NMES, the number of EdU$^+$ nuclei below the basal lamina (i.e., MuSCs and myofiber nuclei) were similarly increased in AMPKα2$^{MuSC\Delta/\Delta}$ mice and controls (Figure 4E), indicating that MuSC activation and proliferation upon NMES are unaffected in absence of AMPKα2. However, their relative contribution to myonuclear accretion was substantially lower after AMPKα2 deletion from MuSCs (Figure 4F), resulting in a blunted increase in the number of PCM1$^+$ myonuclei after NMES (Figure 4G), and a lower percentage of newly acquired myonuclei (Figure 4H). In line with our previous findings,[31] MuSC self-renewal seems to be spared, since the total number of Pax7$^+$ cells, as well as the number of EdU$^+$Pax7$^+$ cells remain unaffected by AMPKα2 deletion (Figures S4H and S4I).

Myofiber-specific AMPKα2 deletion (AMPKα2$^{MF\Delta/\Delta}$) was verified, and resulted in a 60% reduction of AMPKα2 protein abundance in whole muscle (Figures S4J and S4K). Similar to AMPKα2$^{MuSC\Delta/\Delta}$ mice, maximal *in vivo* tetanic force was unaltered in AMPKα2$^{MF\Delta/\Delta}$ mice throughout the stimulation protocol (Figures S4F and S4L). Furthermore, AMPKα2$^{MF\Delta/\Delta}$ mice displayed a similar NMES-induced increase in EdU$^+$ nuclei below the basal lamina compared to controls (Figure S4M). In contrast to AMPKα2$^{MuSC\Delta/\Delta}$ mice, myonuclear accretion was unaffected in AMPKα2$^{MF\Delta/\Delta}$ mice (Figures S4N), showing that AMPKα2 does not play an acute role in the myofiber-specific regulation of myonuclear accretion. Moreover, MuSC maintenance remained unaffected (Figures S4O and S4P).

Together, these data are in line with a MuSC-intrinsic role of AMPKα2 in the regulation of myonuclear accretion *in vivo*, upon myofiber contractions induced by NMES.

DISCUSSION

MuSCs predominantly contribute to skeletal muscle homeostasis by two types of MuSC fusion; MuSC-MuSC fusion and myonuclear accretion. Myonuclear accretion is distinguished by the need for a coordination of cell type specific events between the myofiber and MuSCs, but it had remained unknown if there is a central molecular regulator that coordinates these events. Here, we demonstrate through *in vitro* and *in vivo* cell tracing that AMPKα2 specifically regulates myonuclear accretion in a MuSC-intrinsic manner.

Several previous studies proposed a specific regulation of myonuclear accretion.[21–23,48–54] However, a collective limitation is that they predominantly rely on *in vitro* data, and only one study (Noviello et al.[52]) directly assessed myonuclear accretion *in vivo*. Despite this limitation, published data collectively point toward a role for Ca^{2+} signaling in the distinct regulation of myonuclear accretion. Moreover, they unanimously show a regulation at the site of the myofiber, as Ca^{2+}-dependent activation of CaMKII occurs in MT,[23] Ras homolog family member A and SRF were shown to have a myofiber-intrinsic role,[22,52] and nuclear factor of activated T cells (NFAT) targets IL-4 and stabilin-2 are specifically expressed by MT.[48,53] Thereby, they form a collective evidence that Ca^{2+} signaling contributes to myofiber-intrinsic regulation of myonuclear accretion.

In contrast to Ca^{2+}-dependent activation of CaMKII,[23] AMPKα2 knockout did not alter gene expression of the fusogens *Mymk* and *Mymx*. Furthermore, AMPKα2 has not been reported to interact with mediators of these NFAT-related pathways. Moreover, in contrast to the myofiber-intrinsic regulation of myonuclear accretion observed in these studies, we observed no effect of myofiber-specific AMPKα2 knockout on either *in vitro* or *in vivo* myonuclear accretion. Rather, we showed a specific role of AMPKα2 in MC, which implies that AMPKα2-BAIAP2 signaling provides a distinct mechanism of regulation from NFAT-dependent pathways. Specifically, AMPKα2 promotes fusion through the phosphorylation of BAIAP2 at Ser366, and limitation of actin bundling. This is in line with previous reports demonstrating that BAIAP2 phosphorylation inhibits binding of BAIAP2 to cellular membranes,[44] and that displacement of the EPS8-BAIAP2 complex from membranes counteracts actin bundling and is required for the progression of fusion beyond membrane apposition.[45]

To our knowledge, only one previous study has indicated a myoblast-intrinsic specific regulation of myonuclear accretion, albeit *in vitro*. In this study, Teng et al., used cytoplasmic tracers to show that the formation of dual-labeled MT was impaired in co-cultures with phospholipase D1 (PLD1) knockdown myoblasts, while PLD1 knockdown in MT had no effect.[54] Similar to AMPKα2-BAIAP2 signaling, they find *in vitro* evidence for PLD1 mediated regulation of cell fusion after membrane apposition.[54] Strikingly, AMPK was shown to regulate PLD1 activity through phosphorylation.[55,56] Thus, while speculative, AMPKα2 may more broadly safeguard membrane fusion beyond membrane apposition.

In conclusion, our work reveals AMPKα2 as a novel MuSC-intrinsic physiological regulator of myonuclear accretion. This adds to the cellular mechanisms by which AMPK controls the maintenance of skeletal muscle quality and quantity.[24,57,58] Blunted AMPK signaling is observed upon aging and in patients with metabolic disorders such as metabolic syndrome and COPD,[59–61] which are all conditions linked with impaired whole body metabolism and muscle pathology that may be improved upon AMPK activation. AMPK activation also mitigates pathologies of neuromuscular diseases such as Duchenne muscular dystrophy, spinal muscular atrophy, and myotonic dystrophy type 1.[62] Although technical limitations currently preclude the *in vivo* characterization of myonuclear accretion in these conditions, the identification of AMPKα2 as a regulator of myonuclear accretion may help to understand the pathophysiology and improve treatment of metabolic disorders and neuromuscular diseases.

Limitations of the study

There is a paucity of studies directly assessing myonuclear accretion *in vitro* and *in vivo*, predominantly due to technical limitations. Several studies used cytoplasmic tracers to observe cell content mixing. However, this does not provide a direct measure of the number of nuclei donated to the myofiber (i.e., the rate of myonuclear accretion). Moreover, tracing of nuclei using nuclear fluorescent reporter proteins (e.g., H2B-GFP) proved unsuccessful due to nuclear propagation.[63] To overcome these limitations, we used EdU incorporation to trace MuSC-derived nuclei at the DNA level. However, EdU incorporation occurs during active DNA synthesis, and as such, we only trace

MuSCs that undergo cell division. Although it is unknown if and to what extend MuSCs fuse without prior cell division, it may lead to an underestimation of the effects observed here. Finally, EdU was delivered with drinking water and therefore labeling may be subject to the circadian rhythm.

A recent study poses that myonuclei might not be post-mitotic,[64] which should be confirmed in future studies, but may imply a further underestimation of the observed myonuclear accretion defect. Theoretically, myonuclear accretion is part of a turnover that includes "myonuclear loss." As "myonuclear loss" cannot be directly measured, its rate and relevance is subject of ongoing debate.[65] Potential alterations in the rate of "myonuclear loss" could influence physiological parameters in this study, including the total number of myonuclei per fiber. Nevertheless, the combination of specific *in vitro* and *in vivo* myonuclear accretion assays allowed us to demonstrate that AMPKα2-BAIAP2 signaling specifically regulates myonuclear accretion in a MuSC-intrinsic manner.

STAR★METHODS

Detailed methods are provided in the online version of this paper and include the following:

- KEY RESOURCES TABLE
- RESOURCE AVAILABILITY
  - Lead contact
  - Materials availability
  - Data and code availability
- EXPERIMENTAL MODEL AND STUDY PARTICIPANT DETAILS
  - Animals
  - Primary MuSC culture
- METHOD DETAILS
  - Muscle force measurement and NMES
  - *In vitro* experiments
  - Immunohistochemistry
  - Live cell imaging
  - AMPK activity
  - Verification of AMPKα2 deletion by PCR
  - RT qPCR
  - Western blot
- QUANTIFICATION AND STATISTICAL ANALYSIS

SUPPLEMENTAL INFORMATION

Supplemental information can be found online at https://doi.org/10.1016/j.isci.2023.108343.

ACKNOWLEDGMENTS

This work was supported by Centre National de la Recherche Scientifique, the Association Française Contre les Myopathies-Téléthon (Alliance MyoNeurALP1 and MyoNeurALP2) and the Agence Nationale de la Recherche (ANR JCJC #ANR-22-CE14-0032-01). A.K. was supported by a Kootstra Talent Fellowship (Maastricht University) and a Marie Skłodowska-Curie Individual Fellowship (#896544). A.S. was supported by Fondation pour la Recherche Médicale (#ECO202206015552). L.G. was supported by Ligue Contre le Cancer (#GB/MA/SC 12627).

AUTHOR CONTRIBUTIONS

R.M. designed the study. A.K. and R.M. conceived, performed, and analyzed experiments. M.T., S.B.L., L.G., A.S., C.D., A.F., and P.R. performed and analyzed experiments. A.K. prepared the figures and wrote the manuscript. R.M., M.T., and K.S. provided conceptual input and edited the manuscript. All authors read and approved the manuscript.

DECLARATION OF INTERESTS

The authors declare no competing interests.

Received: January 4, 2023
Revised: July 28, 2023
Accepted: October 23, 2023
Published: October 26, 2023

REFERENCES

1. Zurlo, F., Larson, K., Bogardus, C., and Ravussin, E. (1990). Skeletal muscle metabolism is a major determinant of resting energy expenditure. J. Clin. Invest. *86*, 1423–1427. https://doi.org/10.1172/JCI114857.
2. Severinsen, M.C.K., and Pedersen, B.K. (2020). Muscle–Organ Crosstalk: The Emerging Roles of Myokines. Endocr. Rev. *41*, 594–609. https://doi.org/10.1210/endrev/bnaa016.
3. Moon, S.-S. (2014). Low skeletal muscle mass is associated with insulin resistance, diabetes, and metabolic syndrome in the Korean population: the Korea National Health and Nutrition Examination Survey (KNHANES) 2009-2010. Endocr. J. *61*, 61–70. https://doi.org/10.1507/endocrj.ej13-0244.
4. Tyrovolas, S., Panagiotakos, D., Georgousopoulou, E., Chrysohoou, C., Tousoulis, D., Haro, J.M., and Pitsavos, C. (2020). Skeletal muscle mass in relation to 10 year cardiovascular disease incidence among middle aged and older adults: the ATTICA study. J. Epidemiol. Community Health *74*, 26–31. https://doi.org/10.1136/jech-2019-212268.
5. Spexoto, M.C.B., Ramírez, P.C., de Oliveira Máximo, R., Steptoe, A., de Oliveira, C., and Alexandre, T.d.S. (2022). European Working Group on Sarcopenia in Older People 2010 (EWGSOP1) and 2019 (EWGSOP2) criteria or slowness: which is the best predictor of mortality risk in older adults? Age Ageing *51*, afac164. https://doi.org/10.1093/ageing/afac164.
6. Wang, D.X.M., Yao, J., Zirek, Y., Reijnierse, E.M., and Maier, A.B. (2020). Muscle mass, strength, and physical performance predicting activities of daily living: a meta-analysis. J. Cachexia Sarcopenia Muscle *11*, 3–25. https://doi.org/10.1002/jcsm.12502.
7. Dumont, N.A., Bentzinger, C.F., Sincennes, M., and Rudnicki, M.A. (2015). Satellite Cells and Skeletal Muscle Regeneration. In Comprehensive Physiology (Wiley), pp. 1027–1059. https://doi.org/10.1002/cphy.c140068.
8. Hardy, D., Besnard, A., Latil, M., Jouvion, G., Briand, D., Thépenier, C., Pascal, Q., Guguin, A., Gayraud-Morel, B., Cavaillon, J.-M., et al. (2016). Comparative Study of Injury Models for Studying Muscle Regeneration in Mice. PLoS One *11*, e0147198. https://doi.org/10.1371/journal.pone.0147198.
9. Mackey, A.L., and Kjaer, M. (2017). The breaking and making of healthy adult human skeletal muscle *in vivo*. Skelet. Muscle *7*, 24. https://doi.org/10.1186/s13395-017-0142-x.
10. Ciciliot, S., and Schiaffino, S. (2010). Regeneration of Mammalian Skeletal Muscle: Basic Mechanisms and Clinical Implications. Curr. Pharm. Des. *16*, 906–914. https://doi.org/10.2174/138161210790883453.
11. Goh, Q., Song, T., Petrany, M.J., Cramer, A.A., Sun, C., Sadayappan, S., Lee, S.-J., and Millay, D.P. (2019). Myonuclear accretion is a determinant of exercise-induced remodeling in skeletal muscle. Elife *8*, e44876. https://doi.org/10.7554/eLife.44876.
12. Murach, K.A., Fry, C.S., Dupont-Versteegden, E.E., McCarthy, J.J., and Peterson, C.A. (2021). Fusion and beyond: Satellite cell contributions to loading-induced skeletal muscle adaptation. FASEB J *35*, e21893. https://doi.org/10.1096/fj.202101096R.
13. Englund, D.A., Murach, K.A., Dungan, C.M., Figueiredo, V.C., Vechetti, I.J., Dupont-Versteegden, E.E., McCarthy, J.J., and Peterson, C.A. (2020). Depletion of resident muscle stem cells negatively impacts running volume, physical function, and muscle fiber hypertrophy in response to lifelong physical activity. Am. J. Physiol. Physiol. *318*, C1178–C1188. https://doi.org/10.1152/ajpcell.00090.2020.
14. Keefe, A.C., Lawson, J.A., Flygare, S.D., Fox, Z.D., Colasanto, M.P., Mathew, S.J., Yandell, M., and Kardon, G. (2015). Muscle stem cells contribute to myofibres in sedentary adult mice. Nat. Commun. *6*, 7087. https://doi.org/10.1038/ncomms8087.
15. Fry, C.S., Lee, J.D., Mula, J., Kirby, T.J., Jackson, J.R., Liu, F., Yang, L., Mendias, C.L., Dupont-Versteegden, E.E., McCarthy, J.J., and Peterson, C.A. (2015). Inducible depletion of satellite cells in adult, sedentary mice impairs muscle regenerative capacity without affecting sarcopenia. Nat. Med. *21*, 76–80. https://doi.org/10.1038/nm.3710.
16. Lehka, L., and Rędowicz, M.J. (2020). Mechanisms regulating myoblast fusion: A multilevel interplay. Semin. Cell Dev. Biol. *104*, 81–92. https://doi.org/10.1016/J.SEMCDB.2020.02.004.
17. Zhang, Q., Vashisht, A.A., O'Rourke, J., Corbel, S.Y., Moran, R., Romero, A., Miraglia, L., Zhang, J., Durrant, E., Schmedt, C., et al. (2017). The microprotein Minion controls cell fusion and muscle formation. Nat. Commun. *8*, 15664. https://doi.org/10.1038/ncomms15664.
18. Quinn, M.E., Goh, Q., Kurosaka, M., Gamage, D.G., Petrany, M.J., Prasad, V., and Millay, D.P. (2017). Myomerger induces fusion of non-fusogenic cells and is required for skeletal muscle development. Nat. Commun. *8*, 15665. https://doi.org/10.1038/ncomms15665.
19. Millay, D.P., O'Rourke, J.R., Sutherland, L.B., Bezprozvannaya, S., Shelton, J.M., Bassel-Duby, R., and Olson, E.N. (2013). Myomaker is a membrane activator of myoblast fusion and muscle formation. Nature *499*, 301–305. https://doi.org/10.1038/nature12343.
20. Bi, P., Ramirez-Martinez, A., Li, H., Cannavino, J., McAnally, J.R., Shelton, J.M., Sánchez-Ortiz, E., Bassel-Duby, R., and Olson, E.N. (2017). Control of muscle formation by the fusogenic micropeptide myomixer. Science *356*, 323–327. https://doi.org/10.1126/science.aam9361.
21. Hindi, S.M., Shin, J., Gallot, Y.S., Straughn, A.R., Simionescu-Bankston, A., Hindi, L., Xiong, G., Friedland, R.P., and Kumar, A. (2017). MyD88 promotes myoblast fusion in a cell-autonomous manner. Nat. Commun. *8*, 1624. https://doi.org/10.1038/s41467-017-01866-w.
22. Guerci, A., Lahoute, C., Hébrard, S., Collard, L., Graindorge, D., Favier, M., Cagnard, N., Batonnet-Pichon, S., Précigout, G., Garcia, L., et al. (2012). Srf-dependent paracrine signals produced by myofibers control satellite cell-mediated skeletal muscle hypertrophy. Cell Metab. *15*, 25–37. https://doi.org/10.1016/j.cmet.2011.12.001.
23. Eigler, T., Zarfati, G., Amzallag, E., Sinha, S., Segev, N., Zabary, Y., Zaritsky, A., Shakked, A., Umansky, K.-B., Schejter, E.D., et al. (2021). ERK1/2 inhibition promotes robust myotube growth via CaMKII activation resulting in myoblast-to-myotube fusion. Dev. Cell *56*, 3349–3363.e6. https://doi.org/10.1016/J.DEVCEL.2021.11.022.
24. Mounier, R., Théret, M., Lantier, L., Foretz, M., and Viollet, B. (2015). Expanding roles for AMPK in skeletal muscle plasticity. Trends Endocrinol. Metab. *26*, 275–286. https://doi.org/10.1016/j.tem.2015.02.009.
25. Battey, E., Furrer, R., Ross, J., Handschin, C., Ochala, J., and Stroud, M.J. (2022). PGC-1α regulates myonuclear accretion after moderate endurance training. J. Cell. Physiol. *237*, 696–705. https://doi.org/10.1002/jcp.30539.
26. Bess, E., Fisslthaler, B., Frömel, T., and Fleming, I. (2011). Nitric Oxide-Induced Activation of the AMP-Activated Protein Kinase α2 Subunit Attenuates IκB Kinase Activity and Inflammatory Responses in Endothelial Cells. PLoS One *6*, e20848. https://doi.org/10.1371/journal.pone.0020848.
27. Wozniak, A.C., and Anderson, J.E. (2009). The dynamics of the nitric oxide release-transient from stretched muscle cells. Int. J. Biochem. Cell Biol. *41*, 625–631. https://doi.org/10.1016/J.BIOCEL.2008.07.005.
28. Sibisi, N.C., Snyman, C., Myburgh, K.H., and Niesler, C.U. (2022). Evaluating the role of nitric oxide in myogenesis *in vitro*. Biochimie *196*, 216–224. https://doi.org/10.1016/J.BIOCHI.2021.11.006.
29. Jørgensen, S.B., Treebak, J.T., Viollet, B., Schjerling, P., Vaulont, S., Wojtaszewski, J.F.P., and Richter, E.A. (2007). Role of AMPKα2 in basal, training-, and AICAR-induced GLUT4, hexokinase II, and mitochondrial protein expression in mouse muscle. Am. J. Physiol. Metab. *292*, E331–E339. https://doi.org/10.1152/ajpendo.00243.2006.
30. McKellar, D.W., Walter, L.D., Song, L.T., Mantri, M., Wang, M.F.Z., De Vlaminck, I., and Cosgrove, B.D. (2021). Large-scale integration of single-cell transcriptomic data captures transitional progenitor states in mouse skeletal muscle regeneration. Commun. Biol. *4*, 1280. https://doi.org/10.1038/s42003-021-02810-x.
31. Theret, M., Gsaier, L., Schaffer, B., Juban, G., Ben Larbi, S., Weiss-Gayet, M., Bultot, L., Collodet, C., Foretz, M., Desplanches, D., et al. (2017). AMPKα1-LDH pathway regulates muscle stem cell self-renewal by controlling metabolic homeostasis. EMBO J. *36*, 1946–1962. https://doi.org/10.15252/embj.201695273.
32. Xiao, B., Sanders, M.J., Carmena, D., Bright, N.J., Haire, L.F., Underwood, E., Patel, B.R., Heath, R.B., Walker, P.A., Hallen, S., et al. (2013). Structural basis of AMPK regulation by small molecule activators. Nat. Commun. *4*, 3017. https://doi.org/10.1038/ncomms4017.
33. Bultot, L., Jensen, T.E., Lai, Y.-C., Madsen, A.L.B., Collodet, C., Kviklyte, S., Deak, M., Yavari, A., Foretz, M., Ghaffari, S., et al. (2016). Benzimidazole derivative small-molecule 991 enhances AMPK activity and glucose uptake induced by AICAR or contraction in skeletal muscle. Am. J. Physiol. Metab. *311*, E706–E719. https://doi.org/10.1152/ajpendo.00237.2016.
34. Relaix, F., Bencze, M., Borok, M.J., Der Vartanian, A., Gattazzo, F., Mademtzoglou, D., Perez-Diaz, S., Prola, A., Reyes-Fernandez, P.C., Rotini, A., and Taglietti, , 5th. (2021). Perspectives on skeletal muscle stem cells. Nat. Commun. *12*, 692. https://doi.org/10.1038/s41467-020-20760-6.

35. Saclier, M., Yacoub-Youssef, H., Mackey, A.L., Arnold, L., Ardjoune, H., Magnan, M., Sailhan, F., Chelly, J., Pavlath, G.K., Mounier, R., et al. (2013). Differentially Activated Macrophages Orchestrate Myogenic Precursor Cell Fate During Human Skeletal Muscle Regeneration. Stem Cell. *31*, 384–396. https://doi.org/10.1002/stem.1288.
36. Rochlin, K., Yu, S., Roy, S., and Baylies, M.K. (2010). Myoblast fusion: When it takes more to make one. Dev. Biol. *341*, 66–83. https://doi.org/10.1016/J.YDBIO.2009.10.024.
37. Abmayr, S.M., and Pavlath, G.K. (2012). Myoblast fusion: lessons from flies and mice. Development *139*, 641–656. https://doi.org/10.1242/dev.068353.
38. Hindi, S.M., Tajrishi, M.M., and Kumar, A. (2013). Signaling mechanisms in mammalian myoblast fusion. Sci. Signal. *6*, re2. https://doi.org/10.1126/scisignal.2003832.
39. Banko, M.R., Allen, J.J., Schaffer, B.E., Wilker, E.W., Tsou, P., White, J.L., Villén, J., Wang, B., Kim, S.R., Sakamoto, K., et al. (2011). Chemical genetic screen for AMPKα2 substrates uncovers a network of proteins involved in mitosis. Mol. Cell *44*, 878–892. https://doi.org/10.1016/j.molcel.2011.11.005.
40. Schaffer, B.E., Levin, R.S., Hertz, N.T., Maures, T.J., Schoof, M.L., Hollstein, P.E., Benayoun, B.A., Banko, M.R., Shaw, R.J., Shokat, K.M., and Brunet, A. (2015). Identification of AMPK Phosphorylation Sites Reveals a Network of Proteins Involved in Cell Invasion and Facilitates Large-Scale Substrate Prediction. Cell Metab. *22*, 907–921. https://doi.org/10.1016/j.cmet.2015.09.009.
41. Misra, A., George, B., Rajmohan, R., Jain, N., Wong, M.H., Kambadur, R., and Thanabalu, T. (2012). Insulin receptor substrate protein 53kDa (IRSp53) is a negative regulator of myogenic differentiation. Int. J. Biochem. Cell Biol. *44*, 928–941. https://doi.org/10.1016/j.biocel.2012.02.020.
42. Lakshman Kumar, P., Wilson, A.C., Rocco, A., Cho, M.H., Wan, E., Hobbs, B.D., Washko, G.R., Ortega, V.E., Christenson, S.A., Li, X., et al. (2021). Genetic variation in genes regulating skeletal muscle regeneration and tissue remodelling associated with weight loss in chronic obstructive pulmonary disease. J. Cachexia Sarcopenia Muscle *12*, 1803–1817. https://doi.org/10.1002/jcsm.12782.
43. Sanders, K.J.C., Kneppers, A.E.M., van de Bool, C., Langen, R.C.J., and Schols, A.M.W.J. (2016). Cachexia in chronic obstructive pulmonary disease: new insights and therapeutic perspective. J. Cachexia Sarcopenia Muscle *7*, 5–22. https://doi.org/10.1002/jcsm.12062.
44. Kast, D.J., and Dominguez, R. (2019). Mechanism of IRSp53 inhibition by 14-3-3. Nat. Commun. *10*, 483. https://doi.org/10.1038/s41467-019-08317-8.
45. Rodríguez-Pérez, F., Manford, A.G., Pogson, A., Ingersoll, A.J., Martínez-González, B., and Rape, M. (2021). Ubiquitin-dependent remodeling of the actin cytoskeleton drives cell fusion. Dev. Cell *56*, 588–601.e9. https://doi.org/10.1016/j.devcel.2021.01.016.
46. Cutler, A.A., Pawlikowski, B., Wheeler, J.R., Dalla Betta, N., Elston, T., O'Rourke, R., Jones, K., and Olwin, B.B. (2022). The regenerating skeletal muscle niche drives satellite cell return to quiescence. iScience *25*, 104444. https://doi.org/10.1016/J.ISCI.2022.104444.
47. Zavoriti, A., Fessard, A., Rahmati, M., Del Carmine, P., Chazaud, B., and Gondin, J. (2021). Individualized isometric neuromuscular electrical stimulation training promotes myonuclear accretion in mouse skeletal muscle. bioRxiv *2021*. 12.14.472254. https://doi.org/10.1101/2021.12.14.472254.
48. Horsley, V., Jansen, K.M., Mills, S.T., and Pavlath, G.K. (2003). IL-4 acts as a myoblast recruitment factor during mammalian muscle growth. Cell *113*, 483–494. https://doi.org/10.1016/s0092-8674(03)00319-2.
49. Horsley, V., Friday, B.B., Matteson, S., Kegley, K.M., Gephart, J., and Pavlath, G.K. (2001). Regulation of the growth of multinucleated muscle cells by an NFATC2-dependent pathway. J. Cell Biol. *153*, 329–338. https://doi.org/10.1083/jcb.153.2.329.
50. Shen, W., Prisk, V., Li, Y., Foster, W., and Huard, J. (2006). Inhibited skeletal muscle healing in cyclooxygenase-2 gene-deficient mice: the role of PGE_2 and $PGF_{2\alpha}$. J. Appl. Physiol. *101*, 1215–1221. https://doi.org/10.1152/japplphysiol.01331.2005.
51. Horsley, V., and Pavlath, G.K. (2003). Prostaglandin F2(alpha) stimulates growth of skeletal muscle cells via an NFATC2-dependent pathway. J. Cell Biol. *161*, 111–118. https://doi.org/10.1083/jcb.200208085.
52. Noviello, C., Kobon, K., Delivry, L., Guilbert, T., Britto, F., Julienne, F., Maire, P., Randrianarison-Huetz, V., and Sotiropoulos, A. (2022). RhoA within myofibers controls satellite cell microenvironment to allow hypertrophic growth. iScience *25*, 103616. https://doi.org/10.1016/j.isci.2021.103616.
53. Park, S.-Y., Yun, Y., Lim, J.-S., Kim, M.-J., Kim, S.-Y., Kim, J.-E., and Kim, I.-S. (2016). Stabilin-2 modulates the efficiency of myoblast fusion during myogenic differentiation and muscle regeneration. Nat. Commun. *7*, 10871. https://doi.org/10.1038/ncomms10871.
54. Teng, S., Stegner, D., Chen, Q., Hongu, T., Hasegawa, H., Chen, L., Kanaho, Y., Nieswandt, B., Frohman, M.A., and Huang, P. (2015). Phospholipase D1 facilitates second-phase myoblast fusion and skeletal muscle regeneration. Mol. Biol. Cell *26*, 506–517. https://doi.org/10.1091/mbc.E14-03-0802.
55. Kim, J.H., Park, J.-M., Yea, K., Kim, H.W., Suh, P.-G., and Ryu, S.H. (2010). Phospholipase D1 mediates AMP-activated protein kinase signaling for glucose uptake. PLoS One *5*, e9600. https://doi.org/10.1371/journal.pone.0009600.
56. Mukhopadhyay, S., Saqcena, M., Chatterjee, A., Garcia, A., Frias, M.A., and Foster, D.A. (2015). Reciprocal regulation of AMP-activated protein kinase and phospholipase D. J. Biol. Chem. *290*, 6986–6993. https://doi.org/10.1074/jbc.M114.622571.
57. Mounier, R., Lantier, L., Leclerc, J., Sotiropoulos, A., Foretz, M., and Viollet, B. (2011). Antagonistic control of muscle cell size by AMPK and mTORC1. Cell Cycle *10*, 2640–2646. https://doi.org/10.4161/cc.10.16.17102.
58. Kjøbsted, R., Hingst, J.R., Fentz, J., Foretz, M., Sanz, M.-N., Pehmøller, C., Shum, M., Marette, A., Mounier, R., Treebak, J.T., et al. (2018). AMPK in skeletal muscle function and metabolism. FASEB J *32*, 1741–1777. https://doi.org/10.1096/fj.201700442R.
59. Salminen, A., and Kaarniranta, K. (2012). AMP-activated protein kinase (AMPK) controls the aging process via an integrated signaling network. Ageing Res. Rev. *11*, 230–241. https://doi.org/10.1016/J.ARR.2011.12.005.
60. Natanek, S.A., Gosker, H.R., Slot, I.G.M., Marsh, G.S., Hopkinson, N.S., Moxham, J., Kemp, P.R., Schols, A.M.W.J., and Polkey, M.I. (2013). Pathways associated with reduced quadriceps oxidative fibres and endurance in COPD. Eur. Respir. J. *41*, 1275–1283. https://doi.org/10.1183/09031936.00098412.
61. Layne, A.S., Nasrallah, S., South, M.A., Howell, M.E.A., McCurry, M.P., Ramsey, M.W., Stone, M.H., and Stuart, C.A. (2011). Impaired muscle AMPK activation in the metabolic syndrome may attenuate improved insulin action after exercise training. J. Clin. Endocrinol. Metab. *96*, 1815–1826. https://doi.org/10.1210/jc.2010-2532.
62. Dial, A.G., Ng, S.Y., Manta, A., and Ljubicic, V. (2018). The Role of AMPK in Neuromuscular Biology and Disease. Trends Endocrinol. Metab. *29*, 300–312. https://doi.org/10.1016/j.tem.2018.02.010.
63. Masschelein, E., D'Hulst, G., Zvick, J., Hinte, L., Soro-Arnaiz, I., Gorski, T., von Meyenn, F., Bar-Nur, O., and De Bock, K. (2020). Exercise promotes satellite cell contribution to myofibers in a load-dependent manner. Skelet. Muscle *10*, 21. https://doi.org/10.1186/s13395-020-00237-2.
64. Borowik, A.K., Davidyan, A., Peelor, F.F., Voloviceva, E., Doidge, S.M., Bubak, M.P., Mobley, C.B., Mccarthy, J.J., Dupont-Versteegden, E.E., and Miller, B.F. (2023). Skeletal Muscle Nuclei in Mice are not Post-mitotic. FUNCTION *4*, zqac059. https://doi.org/10.1093/function/zqac059.
65. Kirby, T.J., and Dupont-Versteegden, E.E. (2022). Cross Talk proposal: Myonuclei are lost with ageing and atrophy. J. Physiol. *600*, 2077–2080. https://doi.org/10.1113/JP282380.
66. Viollet, B., Andreelli, F., Jørgensen, S.B., Perrin, C., Geloen, A., Flamez, D., Mu, J., Lenzner, C., Baud, O., Bennoun, M., et al. (2003). The AMP-activated protein kinase alpha2 catalytic subunit controls whole-body insulin sensitivity. J. Clin. Invest. *111*, 91–98. https://doi.org/10.1172/JCI16567.
67. Lepper, C., Conway, S.J., and Fan, C.-M. (2009). Adult satellite cells and embryonic muscle progenitors have distinct genetic requirements. Nature *460*, 627–631. https://doi.org/10.1038/nature08209.
68. Schuler, M., Ali, F., Metzger, E., Chambon, P., and Metzger, D. (2005). Temporally controlled targeted somatic mutagenesis in skeletal muscles of the mouse. genesis *41*, 165–170. https://doi.org/10.1002/gene.20107.
69. Liu, L., Cheung, T.H., Charville, G.W., and Rando, T.A. (2015). Isolation of skeletal muscle stem cells by fluorescence-activated cell sorting. Nat. Protoc. *10*, 1612–1624. https://doi.org/10.1038/nprot.2015.110.
70. Vignaud, A., Cebrian, J., Martelly, I., Caruelle, J.-P., and Ferry, A. (2005). Effect of anti-inflammatory and antioxidant drugs on the long-term repair of severely injured mouse skeletal muscle. Exp. Physiol. *90*, 487–495. https://doi.org/10.1113/expphysiol.2005.029835.

STAR★METHODS

KEY RESOURCES TABLE

REAGENT or RESOURCE	SOURCE	IDENTIFIER
Antibodies		
Anti CD45-PE	Invitrogen	Cat#12-5981-82; Clone 30-F11
Anti CD31-PE	Invitrogen	Cat#12-5981-82; Clone 390
Anti Sca1-PE	Invitrogen	Cat#12-5981-82; Clone D7
Anti CD34-FITC	Invitrogen	Cat#11-0341-85; Clone RAM34
Anti α7integrin-647	AbLab	Cat#67-0010-05; Clone R2F2
embryonic Myosin Heavy Chain (eMyHC)	Santa Cruz	Cat#sc-53091
Laminin α1 (Laminin)	Sigma-Aldrich	Cat#L9393
Pericentriolar Material 1 (PCM1)	Sigma-Aldrich	Cat#HPA023370
Laminin α2 (Laminin)	Santa Cruz	Cat#sc-59854
Paired Box 7 (Pax7)	DSHB	Cat#AB_528428
Myogenin (MyoG)	Santa Cruz	Cat#SC-12732
Desmin	Abcam	Cat#Ab32362
FLAG M2	Sigma	Cat#F3165
Laminin α1 (Laminin)	Sigma-Aldrich	Cat#L9393
Pericentriolar Material 1 (PCM1)	Sigma-Aldrich	Cat#HPA023370
anti AMPKα2	a kind gift from G. Hardie, University of Dundee, Scotland	N/A
Paired Box 7 (Pax7)	DSHB	Cat#AB_528428
Myogenin (MyoG)	Santa Cruz	Cat#SC-12732
Desmin	Abcam	Cat#Ab32362
FLAG M2	Sigma	Cat#F3165
Chemicals, peptides, and recombinant proteins		
Tamoxifen (TX)	MP Biochemicals	Cat#0215673891
Cardiotoxin (CTX)	Latoxan	Cat#L8102
5 ethynyl 2′ deoxyuridine (EdU)	Carbosynth	Cat#NE0870
Collagenase II	Gibco	Cat#17101015
Dispase	Gibco	Cat#17105041
ACK Lysis Buffer	Lonza	Cat#10548E
Matrigel	Corning	Cat#354234
DMEM F12	Gibco	Cat#31331028
Foetal Bovine Serum (FBS)	Gibco	Cat#10270106
Ultroser G	PALL life sciences	Cat#15950017
Penicillin/Streptomycin (PS)	Gibco	Cat#15140122
Gelatin	Sigma-Aldrich	Cat#G1393
Horse Serum (HS)	Gibco	Cat#16050130
Compound 991 (ex229)	Selleckchem	Cat#S8654
Lipofectamine 2000	Invitrogen	Cat#11668019
Tragacanth gum	VWR	Cat#ICNA0210479280
Hoechst	Sigma-Aldrich	Cat#14533
Fluoromount G	Interchim	Cat#FP-483331
CellTracker Deep Red	ThermoFisher	Cat#C34565

(*Continued on next page*)

Continued

REAGENT or RESOURCE	SOURCE	IDENTIFIER
REDExtract N Amp PCR ReadyMix	Sigma-Aldrich	Cat#R4775
TRIzol reagent	Invitrogen	Cat#15596026
Superscript II Reverse Transcriptase	Invitrogen	Cat#18064022
LightCycler 480 SYBR Green I Master	Roche	Cat#04887352001
Protease inhibitor cocktail	Sigma-Aldrich	Cat#P8340
Critical commercial assays		
Satellite Cell Isolation Kit	Miltenyi Biotec	Cat#130104268
Click-iT EdU HCS Assay	Invitrogen	Cat#C10350 / Cat#C10356
Q5 Site-Directed Mutagenesis Kit	New England BioLabs	Cat#E0554S
G-actin/F-actin *in vivo* Assay Kit	Cytoskeleton	Cat#BK037
Pierce ECL Western Blotting Substrate	Thermo Scientific	Cat#32109
Supersignal West FEMTO Chemiluminescent Substrate	Thermo Scientific	Cat#34096
Experimental models: Organisms/strains		
AMPK$\alpha 2^{-/-}$ mice	Mice were kindly provided by Benoit Viollet	N/A
AMPK$\alpha 2^{fl/fl}$ mice	Mice were kindly provided by Benoit Viollet	N/A
Pax7CreER^{T2} mice	The Jackson Laborarory	Cat#012476; RRID:IMSR_JAX:012476
HSACreER^{T2} mice	Mice were kindly provided by Daniel Metzger	N/A
Oligonucleotides		
PCR primer AMPKα2 wt/floxed allele Rev: GTC TTC ACT GAA ATA CAT AGC A	This paper	N/A
PCR primer AMPKα2 null allele Rev: GCA TTG AAC CAC AGT CCT TCC TC	This paper	N/A
Primer Fw Cyclophilin (PPI): GTG ACT TTA CAC GCC ATA ATG	This paper	N/A
Primer Rev Cyclophilin (PPI):ACA AGA TGC CAG GAC CTG TAT	This paper	N/A
Primer Fw Ribosomal protein lateral stalk subunit P0 (RPLP0): ATC GTC TTT AAA CCC CGC GT	This paper	N/A
Primer Rev Ribosomal protein lateral stalk subunit P0 (RPLP0): ACG TTG TCT GCT CCC ACA AT	This paper	N/A
Primer Fw Beta-2-microglobulin (B2M): CAC ATG TCT CGA TCC CAG	This paper	N/A
Primer Rev Beta-2-microglobulin (B2M): CAG TTC CAC CCG CCT CAC	This paper	N/A
Primer Fw AMPKα2 (Prkaa2): CCG AGG GGG TGT GTT TTA CA	This paper	N/A
Primer Rev AMPKα2 (Prkaa2): TGA TAG TCG CTC GCT TCA GG	This paper	N/A
Primer Fw Myogenin (MyoG): CAG CCC AGC GAG GGA ATT TA	This paper	N/A
Primer Rev Myogenin (MyoG): AGA AGC TCC TGA GTT TGC CC	This paper	N/A
Primer Fw Myomaker (Mymk): CAT CGC TGT GCG GAC TTT TC	This paper	N/A

(*Continued on next page*)

Continued

REAGENT or RESOURCE	SOURCE	IDENTIFIER
Primer Rev Myomaker (Mymk): TGT AGA TGC TCT TGT CGG GG	This paper	N/A
Primer Fw Myomixer (Mymx): GGC CGG TTA GAA CTG GTG AG	This paper	N/A
Primer Rev Myomixer (Mymx): AAG CAC CAT CGG GAG CAA TG	This paper	N/A
Primer Fw BAR/IMD domain containing adaptor protein 2 (Baiap2): TCA GGC TGA GCT GAA GAA GC	This paper	N/A
Primer Rev BAR/IMD domain containing adaptor protein 2 (Baiap2): AGT GCT GTC TTG TAG CCG TC	This paper	N/A
Recombinant DNA		
Plasmid pECE M2 BAIAP2 WT	Addgene	Cat#31656, RRID:Addgene_31656
Plasmid pECE M2 BAIAP2 S366A	Addgene	Cat#31657, RRID:Addgene_31657
Plasmid pECE M2 BAIAP2 S366E	This paper	N/A
Plasmid pECE M2 BAIAP2 S366D	This paper	N/A

RESOURCE AVAILABILITY

Lead contact

Further information and requests for resources and reagents should be directed to and will be fulfilled by the lead contact, Rémi Mounier (remi.mounier@univ-lyon1.fr).

Materials availability

Plasmids generated in this study will be made available upon request.

Data and code availability

- All data reported in this paper will be shared by the lead contact upon request.
- This paper does not report original code.
- Any additional information required to reanalyze the data reported in this paper is available from the lead contact upon request.

EXPERIMENTAL MODEL AND STUDY PARTICIPANT DETAILS

Animals

Mice were bred, housed and maintained in accordance with the French and European legislation. The experimental protocols were approved by the local ethical committee. Experiments were conducted on males at 8-12 weeks of age. Mice were genotyped by PCR using toe or tail DNA. AMPKα2 mice were used for MuSC extraction and *in vivo* experiments.[66] Pax7Cre;AMPKα2$^{fl/fl}$ were obtained by crossing Pax7CreER$^{T2/+}$ mice[67] with AMPKα2$^{fl/fl}$ mice.[57] Similarly HSACre;AMPKα2$^{fl/fl}$ were obtained by crossing HSACreER$^{T2/+}$ mice[68] with AMPKα2$^{fl/fl}$ mice. Activation of Cre activity in CreER^{T2} mice was induced by daily intraperitoneal (i.p.) Tamoxifen (0.1mg/g BW in sunflower oil) injections for 4 days. Subsequent experiments were initiated 1 week (*i.e.*, for regeneration experiment) or 3 weeks (*i.e.*, for NMES) after the first Tamoxifen injection. Skeletal muscle injury was induced by Cardiotoxin (CTX) injection in the *tibialis anterior* (TA) (50µl per TA, 12µM). Mice were fed 5 ethynyl 2′ deoxyuridine (EdU) in the drinking water (0.5 mg/ml, 1% glucose) at indicated timepoints and durations to label and trace activated MuSCs.

Primary MuSC culture

MuSCs were isolated from hindlimb muscles of age-matched male AMPKα2$^{+/+}$ and AMPKα2$^{-/-}$ mice at 8-12 weeks of age, using an adaptation of published methods.[31,69] Briefly, muscles were dissected and digested with Collagenase II and Dispase.[69] Dissociated muscles were passed through a 70µm filter and red blood cells were lysed in ACK lysis buffer. Cell suspensions were then incubated with anti CD45, anti CD31, anti Sca1, anti CD34, and anti α7integrin, and CD45/CD31/Sca1^{-};CD34/α7int^{+} were sorted using a BD FACSAria II cytometer (FACS).[31]

Alternatively, cell suspensions were incubated with Satellite Cell Isolation Kit for non MuSC depletion by magnetic activated cell sorting (MACS). MuSC purity after MACS was verified by Desmin IHC to be at 94±3% (mean±SD).

FACS isolated MuSCs were seeded onto Matrigel coated supports at 3000 cells/cm^2, and amplified during 5 days in proliferation medium (DMEM F12, 20% Foetal Bovine Serum (FBS), 2% Ultroser G, and 1% Penicillin/Streptomycin (PS). Proliferation medium was replaced at day 3 of amplification.

MACS isolated MuSCs were seeded onto Gelatin coated supports at 3000 cells/cm^2, and amplified $\leq$3 passages in proliferation medium. Only experiments with transfected cells (Figures 3H–3J and S3G-K) and Figure 3K were conducted using MACS-isolated MuSCs.

METHOD DETAILS

Muscle force measurement and NMES

In situ muscle force production was assessed as described previously.[70] Briefly, mice were anaesthetized by i.p. pentobarbital sodium injection (50 mg/kg). The knee and foot were fixed with clamps and stainless-steel pins, and the distal tendon of the TA was cut and attached to an isometric transducer (Harvard Bioscience) using a silk ligature. The sciatic nerves were proximally crushed and distally stimulated by bipolar silver electrode using supramaximal square wave pulses of 0.1 ms duration. Maximal force production was determined in response to isometric contractions induced by 500 ms stimulation trains at 75-150 Hz. To assess fatigue resistance, muscles were stimulated at 20 Hz. Fatigue resistance was expressed as time to reach <70% of initial force.

Myonuclear accretion was invoked by *in vivo* individualized non-damaging neuromuscular electrical stimulation (NMES) of the mouse plantar flexor muscles under isoflurane aneasthesia.[47] Briefly, mice were subjected to 2*3 consecutive days of NMES consisting of 80 stimulation trains at 50 Hz (2 s duration, 8 s recovery) at a current intensity resulting in 15% of maximal isometric force production (Fmax). Fmax was measured in response to a 250 ms stimulation train at 100 Hz. Mice were sacrificed after an Fmax test, 24 hr after the last NMES session.

In vitro experiments

After amplification, MuSC progeny (*i.e.*, myoblasts) were trypsinized and plated at indicated densities onto Matrigel coated supports. To induce differentiation, proliferation medium was removed and replaced by differentiation medium (DMEM F12, 2% Horse serum (HS), and 1 % PS). To trace myoblasts *in vitro*, cells were incubated with EdU (10 μM). To induce AMPK activation, cells were treated with the small molecule compound 991 (10 μM). Myoblasts were transfected with pECE M2 BAIAP2 WT (BAIAP2^{WT}), pECE M2 BAIAP2 S366A (BAIAP2^{S366A}), pECE M2 BAIAP2 S366E (BAIAP2^{S366E}), or pECE M2 BAIAP2 S366D (BAIAP2^{S366D}) using Lipofectamine 2000. Six hours after transfection, cells were induced to differentiate. BAIAP2^{WT} and BAIAP2^{S366A} plasmids were a gift from Anne Brunet. BAIAP2^{S366E} and BAIAP2^{S366D} plasmids were generated using the Q5 Site-Directed Mutagenesis Kit according to the manufacturer's instructions. Plasmids were verified by Sanger sequencing (Mix2Seq, Eurofins).

Immunohistochemistry

For immunohistochemical analyses, muscles of interest were isolated, embedded in tragacanth gum, frozen in liquid nitrogen cooled isopentane, and stored at -80°C until use. 10 μm-thick cryosections were prepared for hematoxylin-eosin (HE) staining and immunolabeling. HE staining was used to assess the efficiency of CTX injections, and muscles were only kept for further analyses if $\geq$75% of the muscle area consisted of centrally nucleated fibers. For immunolabeling, cryosections were permeabilized for 10 min in 0.5% Triton X-100 in PBS and saturated in 2% BSA for 1 hr at room temperature (RT). For identification of regenerating myofibers, sections were co-labelled overnight at 4°C with primary antibodies directed against embryonic Myosin Heavy Chain (eMyHC; 1:100) and Laminin α1 (1:200). For identification of myofiber nuclei, sections were co-labelled with primary antibodies directed against Pericentriolar Material 1 (PCM1; 1:1000) and Laminin α2 (1:1000). For identification of MuSCs, sections were fixed for 20 min in 4% paraformaldehyde (PFA) at RT, and permeabilized for 6 min in 100% methanol at -20°C. After antigen retrieval for 2*5 min in 10 mM Citrate buffer at 90°C, sections were saturated in 4% BSA for 2 hr at RT. Sections were then co-labelled overnight at 4°C with primary antibodies directed against Paired Box 7 (Pax7; 1:50) and Laminin α1 (1:100) in 2% BSA. Secondary antibodies were coupled to FITC, Cy3 or Cy5 (Jackson ImmunoResearch Inc.; 1:200) and incubated for 45-60 min at 37°C. Labelling of EdU was performed after secondary antibody incubation using Click-It EdU Kit. Nuclear counterstain was performed by 10 sec incubation with Hoechst (2 μM), and coverslips were mounted with Fluoromount G.

Cultured cells were fixed for 10 min in 4% PFA at RT, permeabilized for 10 min in 0.5% Triton X-100 in PBS, and saturated in 4% BSA for 1 hr at room temperature (RT). Cells were then incubated overnight at 4°C with primary antibodies directed against Myogenin (MyoG; 1:50), Desmin (1:200), and/or FLAG M2 (1:50) in 2% BSA. Secondary antibodies were coupled to FITC, Cy3 or Cy5 (Jackson ImmunoResearch Inc.; 1:200) and incubated for 45-60 min at 37°C. Labelling of EdU was performed after secondary antibody incubation using Click-It EdU Kit. Nuclear counterstain was performed by 10 sec incubation with Hoechst, and cells were covered with Fluoromount G.

Confocal images were acquired at 63x with a Zeiss LSM 880. Images of fluorescent immunolabeling in cell culture supports and scanned slides were acquired with a Zeiss Axio Observer Z1 connected to a Coolsnap HQ2 camera. Scanned slides of PCM1 stainings were acquired with a Zeiss Axio Scan.Z1. Randomly chosen fields of view from sections or cells cultured on removable chamber slides were acquired using a Zeiss Axio Imager Z1 connected to a Coolsnap Myo camera. For each condition of each experiment, at least 5-10 randomly chosen fields of view were counted. The fusion index was calculated as the percentage of nuclei within a cell containing $\geq$2 nuclei. *In vitro* myonuclear accretion was defined as fusion between an EdU-labelled myocyte and a pre-generated myotube ($\geq$2 nuclei), and was calculated as the percentage of EdU$^+$ nuclei within a myotube containing $\geq$2 EdU$^-$ nuclei.

Live cell imaging

Time-lapse imaging of live cells was performed using a Zeiss Axio Observer Z1 connected to a Coolsnap HQ2 camera. For analysis of cell motility, myocytes were captured by brightfield imaging at 5 min intervals. At least 50 cells were tracked in 5-10 individual fields of view covering a total of 3 hr using MetaMorph image analysis software. For analysis of fusion events, cells were captured by brightfield imaging at 15 min intervals. Fusion events of at least 50 myocytes were scored in 5 individual fields of view covering a total of 12 hr. To observe myonuclear accretion, myocytes were labelled with 1 μM CellTracker Deep Red according to the manufacturer instructions, and then co-cultured with 24-hour differentiated unstained myotubes. 12 hr after initiation of co-culture, cells were captured by brightfield and fluorescent imaging at 6.7 min intervals covering a total of 5 hr.

AMPK activity

Skeletal muscle tissue (*TA*) was rapidly harvested from the indicated animals, snap-frozen in liquid nitrogen, and stored at -80°C. The muscles were homogenized in cold lysis buffer, and protein extracts were prepared as previously described.[33] AMPKα2 versus AMPKα1-containing complexes were immunoprecipitated using an anti-AMPKα2 and anti-AMPKα1 antibody, respectively, and *in vitro* phosphotransferase activity was determined towards the AMRA peptide (AMRAASAAALARRR) as previously described.[33]

Verification of AMPKα2 deletion by PCR

To verify MuSC specific deletion of AMPKα2, hindlimb muscles of Tamoxifen treated Pax7Cre;AMPKα2$^{fl/fl}$ mice were collected 3 weeks after the first Tamoxifen injection. MuSCs were extracted by FACS sorting of CD45/CD31/Sca1^{-};CD34/α7int^{+} cells, and CD45/CD31/Sca1^{+} were sorted as non MuSC controls. For HSACre;AMPKα2$^{fl/fl}$ mice, deletion was verified at the end of the experimental protocol in whole muscle cryosections. DNA was extracted in 25 mM NaOH, 0.2 mM EDTA, and neutralized in 40 mM Tris-HCL ph5. Amplification was performed using REDExtract N Amp PCR ReadyMix according to the manufacturer protocol.

RT qPCR

Cells were lysed in TRIzol reagent, and total RNA was obtained by chloroform/isopropanol based extraction according to the manufacturer protocol. RNA was reverse transcribed using Superscript II Reverse Transcriptase, and qPCR was carried out using 1.5 μl of cDNA, 5 μl LightCycler 480 SYBR Green I Master, and 0.5 μl primers (10 μM) at 10 μl total volume. After initial 5 min denaturation at 95°C, amplification was performed at 95°C (10 sec), 60°C (5 sec), 72°C (10 sec) for 45 cycles carried out on a Bio Rad CFX. Relative gene expression was calculated using $2^{-\Delta\Delta Ct}$. Values were normalized to the geometric mean of three reference genes (PPI, RPLP0, and B2M).

Western blot

The ratio between Filamentous (F) and Globular (G) Actin was determined using the G-actin/F-actin *in vivo* Assay Kit. Briefly, lysed cells were cleared by centrifugation (500 *g*, 5 min), and supernatants were centrifuged at 100,000 *g*, 1h at 37°C. The resulting F-actin pallet was solubilized in F-actin depolymerization buffer at a volume equal to that of the G-actin containing supernatant. Equal volumes of G- and F-actin fractions were resolved by SDS-PAGE.

For confirmation of AMPKα2 knockdown, thick cryosections were lysed in AMPK lysis buffer (50 mM Tris-HCL, 1 mM EDTA, 1 mM EGTA, 0.27 mM Sucrose, 1% Triton X-100, 20 mM β-Glycerophosphate disodium salt hydrate, 50 mM NaF, 0.5 mM PMSF, 1 mM Benzamidine, 1 mM DTT, 1 mM Na_3VO_4, and Protease inhibitor cocktail). Tissue was disrupted using a Precellys Evolution Touch homogenizer (Bertin Technologies) and ceramic beads, and sonication (Diagenode Bioruptor Plus Sonicator). Total protein was quantified using BCA Protein Assay Kit, and equal amounts of protein were resolved by SDS-PAGE.

Proteins were transferred to a nitrocellulose membrane, and for total protein detection, the membrane was stained with PonceauS solution and imaged using a ChemiDoc MP imaging system (Bio-Rad). Proteins of interest were detected by AMPKα2 antibody and Anti-Pan Actin antibody, visualized by chemiluminescence using Pierce ECL Western Blotting Substrate or Supersignal West FEMTO Chemiluminescent Substrate, and detected using a ChemiDoc MP imaging system (Bio-Rad).

QUANTIFICATION AND STATISTICAL ANALYSIS

For *in vitro* experiments, replicates signify cells extracted from individual mice. For *in vivo* experiments, replicates signify individual muscles. Normal distribution was approximated from QQ plots. All *in vivo* results were analysed using unpaired parametric analyses, whereas *in vitro* results were analysed using paired parametric analyses. Statistical significance was determined using two-sided Student's *t* tests or Welch's t tests, or ANOVA with Bonferroni *post hoc* analyses in case of multiple comparisons, using GraphPad Prism software version 9.5.0. Time points were compared if specifically indicated. Details can be found in the figures and figure legends.